DMD-AR-2021-000553R1

**Complex Cytochrome P450 kinetics due to multisubstrate binding and sequential**

**metabolism. Part 1. Theoretical considerations.**

Zeyuan Wang*, Erickson M. Paragas*, Swati Nagar, and Ken Korzekwa

Department of Pharmaceutical Sciences, Temple University School of Pharmacy, 3307 N Broad

Street, Philadelphia, Pennsylvania 19140

*These authors contributed equally to the work.

1

DMD-AR-2021-000553R1

**Running Title:**

Complex CYP kinetics: Theoretical Considerations

Address correspondence to: Dr. Ken Korzekwa, 3307 N Broad St. Philadelphia, PA 19140,

215-707-7892, korzekwa@temple.edu

**Number of text pages: 28**

**Number of tables: 1**

**Number of figures: 10**

**Number of references: 62**

**Number of words in**

      **Abstract: 139**

      **Introduction: 825**

      **Discussion: 1641**

**ABBREVIATIONS:**

AICc: corrected Akaike information criterion, $CL_{int}$: intrinsic clearance, CYP: cytochrome P450,

DDI: drug-drug interaction, E: enzyme, EH: Eadie-Hofstee, ES: enzyme-substrate complex,

ESS: enzyme-substrate-substrate complex, EP: enzyme-product complex, ES*: active

oxygenating species derived from ES, ESS*: active oxygenating species derived from ESS, $E_t$:

total enzyme concentration, k: rate constants, $k_{cat}$: catalytic turnover rate, $K_m$: Michaelis-Menten

constant, ODE: ordinary differential equations, P: product, S: substrate, Seq: sequential, $V_{max}$:

maximal velocity

**Keywords**

Numerical methods, Michaelis-Menten, sequential metabolism, multiple substrate binding,

atypical kinetics, cytochrome P450

DMD-AR-2021-000553R1

**Abstract**

Complexities in CYP mediated metabolism kinetics include multisubstrate binding, multiple

product formation and sequential metabolism. Saturation curves and intrinsic clearances were

simulated for single substrate and multisubstrate models using derived velocity equations and

numerical solutions of ordinary differential equations (ODEs). Multisubstrate models focused on

sigmoidal kinetics due to their dramatic impact on clearance predictions. These models were

combined with multiple product formation and sequential metabolism and simulations were

performed with random error. Use of single substrate models to characterize multisubstrate data

can result in inaccurate kinetic parameters and poor clearance predictions. Comparing results for

use of standard velocity equations with ODEs clearly shows that ODEs are more versatile and

provide better parameter estimates. It would be difficult derive concentration-velocity

relationships for complex models, but these relationships can be easily modeled using numerical

methods and ODEs.

**Significance Statement**

The impact of multisubstrate binding, multiple product formation, and sequential metabolism on

the CYP kinetics was investigated. Numerical methods are capable of characterizing complicated

CYP kinetics.

DMD-AR-2021-000553R1

**Introduction**

Drug metabolism plays an important role in determining the pharmacokinetic and pharmacodynamic properties of drug candidates. Cytochrome P450s (CYPs) are a superfamily of enzymes involved in the metabolism of over 70% of drugs currently on the market (Zanger and Schwab, 2013). CYP-mediated clearance and related drug interactions can be a major issue during drug development. CYPs demonstrate unusual kinetics with respect to ligand selectivity (Ekroos and Sjögren, 2006) and multiple-substrate binding. In many cases, multi-substrate binding results in atypical saturation kinetics, including sigmoidal saturation, substrate inhibition, and biphasic saturation curves (Korzekwa et al., 1998; Tracy, 2006). Spectral binding and X-ray crystallography studies support the theory that the active sites of some CYPs are large and flexible (Shou et al., 1994; Ueng et al., 1997; Korzekwa et al., 1998; Hosea et al., 2000; Domanski et al., 2001; Ekins et al., 2003; Yoon et al., 2004) and can accommodate the simultaneous binding of multiple substrates (Li and Poulos, 2004; Wester et al., 2005; Roberts et al., 2011; Nguyen et al., 2016; Sevrioukova and Poulos, 2017). In addition to the simultaneous multiple binding of molecules of the same substrate, binding of different substrates occurs as well, resulting in heterotropic activation and inhibition (Ueng et al., 1997; Kenworthy et al., 2001; Hutzler and Tracy, 2002; Galetin et al., 2003; Collom et al., 2008; Blobaum et al., 2013). There are many possible factors that may be involved in non-Michaelis-Menten CYP kinetics, including active site flexibility, distinct binding sites (Hosea et al., 2000), and protein-protein interactions (Jamakhandi et al., 2007; Davydov et al., 2017; Dangi et al., 2021). However, most experimental saturation curves can be represented adequately by more simple ES and ESS models.

The combination of active site flexibility, fast rotation speed of substrate molecules in the active site, and versatile active oxygen species (Guengerich, 2018), results in multiple metabolite formation in a parallel or sequential manner (Masubuchi et al., 1996; Galetin et al., 2004; Obach, 2013). Multiple primary metabolites formed from the enzyme-substrate (ES) and enzyme-substrate-substrate (ESS) complex (Jones and Korzekwa, 1996) and secondary metabolite formation (Pang, 1995) add more complexity to CYP kinetics. Velocity equations as a function of substrate concentration and initial conditions are not easily derived for these complex schemes.

Since Cleland published methods for the least-squares analysis of enzyme kinetic data in 1979 (Cleland, 1979), there has been a steady movement away from graphical methods for kinetic analyses to robust statistical analyses by model fitting to derived velocity equations (e.g., the Michaelis-Menten equation) and various methods of numerical analysis (Hemker, 1972; Plant, 1979; Frenzen and Maini, 1988; Johnson, 2009; Kuzmič, 2009; Manimozhi et al., 2010; Rajendran et al., 2018; Yadav et al., 2021). For enzyme kinetic models with one independent variable (time) kinetic schemes can be represented as a collection of ordinary differential equations (ODEs). In addition to the derivation and use of velocity equations to model enzyme kinetics, ODEs can be used with numerical methods to directly model and parameterize complex kinetic schemes. The complex CYP kinetics encountered in time-dependent inactivation including inactivator binding, inhibitor depletion and sequential metabolism has been previously modeled using numerical analysis (Korzekwa et al., 2014; Nagar et al., 2014; Yadav et al., 2018; Yadav et al., 2020; Yadav et al., 2021).

CYP kinetics parameters are often used to determine the enzymes responsible for metabolite

formation and to predict the potential for drug-drug interactions. Another commonly used CYP

assay measures substrate depletion over time to estimate the intrinsic clearance (CLint) of a

reaction. This is the first order rate constant observed at low substrate concentrations for most

kinetic schemes. This clearance is then used to scale up to predict drug clearance in humans. It

has been demonstrated that use of a different concentration range may lead to variable in vitro

$CL_{int}$ estimations when sigmoidal kinetics are observed (Komura et al., 2005; Iwaki et al., 2019).

Simulations have shown that $V_{max}/K_m$ will not be accurate when sigmoidal kinetics is observed

and the turnover rate from the ES complex approaches zero (Korzekwa, 2021).

With respect to sequential metabolism and multiple metabolites, numerical solutions have been

reported previously (Frenzen and Maini, 1988; Varón et al., 2005), but no derived velocity

equations have been reported, possibly due to the complex branched pathways that must be

considered. The numerical method is facile for modeling multiple metabolite formation.

Modeling metabolite exposure is a crucial issue in drug discovery and development especially

for active (Obach, 2013) and toxic circulating metabolites (Schadt et al., 2018). Numerical

analysis using ODEs is expected to easily provide accurate parameters for multiple metabolites,

possibly leading to more accurate in vivo predictions of drug metabolism and metabolite

disposition.

In Part 1 of these manuscripts, we demonstrate the use of the numerical analyses in

characterizing $K_m$, $V_{max}$, and concentration-dependent $CL_{int}$ upon multi-substrate binding,

8

describing concentration-dependent metabolite ratios, and investigating sequential metabolism.

In Part 2, in-house data of three different model drugs - midazolam, ticlopidine and diazepam

were generated and analyzed with this modeling strategy.

**Materials and Methods**

**Theoretical Considerations.** Fig. 1A shows the traditional single-substrate binding model, in

which the EP complex is assumed to be short-lived compared to the ES complex. The equation

derived from this scheme is the well-known Michaelis-Menten equation (Michaelis and Menten,

1913).

$$\frac{velocity\ (v)}{E_t} = \frac{\frac{Vmax}{E_t}[S]}{K_m+[S]} = \frac{k_{cat}[S]}{K_m+[S]} \quad (1)$$

Where $k_{cat}$ is the maximum velocity at unit enzyme concentration ($E_t$), [S] is the substrate

concentration, and $K_m$ is the substrate concentration at half-maximum turnover rate. Fig. 1B

shows a two-substrate model, which can result in non-Michaelis-Menten kinetics. Evidence of

non-Michaelis-Menten (atypical) kinetics has been reported widely for many CYPs, reactions,

and substrates (Atkins, 2005; Atkins, 2006). Multiple substrate binding in the enzyme active site

has been confirmed with X-ray crystallography (Yano et al., 2004; Gay et al., 2010). Most

categories of atypical kinetics can be explained by Fig. 1B, where the specific binding

orientation of substrates is not assumed. For these models, the first substrate binds to the enzyme

active site with an apparent $K_{m1} = (k_2+k_3)/k_1$ and turnover rate $k_{cat1} = k_3$. A second substrate

binds to the enzyme active site with an affinity $K_{m2} = (k_5+k_6)/k_4$ and turnover rate $k_{cat2} = k_6$ (Fig.

1C). The $K_m$ values are apparent, since both processes occur simultaneously. Sigmoidal kinetics

can be observed when $K_{m1} > K_{m2}$ or $k_{cat1} < k_{cat2}$. Biphasic kinetics is observed when $K_{m1} < K_{m2}$

and $k_{cat1} < k_{cat2}$. Substrate inhibition occurs at the condition of $K_{m1} < K_{m2}$ and $k_{cat1} > k_{cat2}$.


Due to large and flexible binding pockets and non-specific substrate orientation for some CYPs

(Shou et al., 1994; Ueng et al., 1997; Korzekwa et al., 1998; Hosea et al., 2000; Domanski et al.,

2001; Ekins et al., 2003; Yoon et al., 2004), formation of multiple metabolites by a single CYP is

common (Masubuchi et al., 1996; Galetin et al., 2004; Obach, 2013). Kinetic schemes that

include the formation of two metabolites are shown in Fig. 2. The schemes in Figs. 2A and B can

correctly model the formation of two products when product formation is rate-limiting. However,

for CYPs, oxygen activation is rate-limiting and substrate oxidation is fast (Luthra et al., 2011).

The branch between formation of the two products occurs from the activated oxygen species and

is not rate-limiting within the catalytic cycle (i.e., the branch is product determining but not rate-

limiting). As described below, it is necessary to use the kinetic schemes in Figs. 2C and D to

describe multi product CYP kinetics. In these schemes, ES* and ESS* represent the activated

oxygen species. It should be noted that $K_{m1mP1} = K_{m1,P2}$ and $K_{m2,P1} = K_{m2,P2}$ is assumed since both

products are formed from the same enzyme-substrate complex.

**Dataset simulation.** Saturation curves (velocity versus substrate concentration) were simulated

as follows: 1) constructing ordinary differential equations (ODEs) for the kinetic schemes in

Fig.1 and 2; 2) varying either the dissociation or turnover rate constant; 3) simulating saturation

curve data with or without adding random error; and 4) directly fitting the Michaelis-Menten

equation, ESSP rate equation, and ODEs for the schemes in Fig.1 and 2 to the simulated dataset

and comparing the fitted parameters with those used in the simulation. Simulations were repeated

500 times, and the results were checked to determine convergence and the distribution of

parameter estimates.

All association rate constants (e.g., $k_1$ and $k_4$ in Fig. 1) were set to 270 $\mu M^{-1}$ $min^1$ (Barnaba et al.,

2016). Simulated dissociation rate constants were selected to achieve the $K_{m1}$ and $K_{m2}$ values in

the range of 1-1000 $\mu M$ (Walsky and Obach, 2004), and  turnover rate constants ($k_{cat1}$ and $k_{cat2}$)

were set within the range of 0 - 60 min$^{-1}$. The values were chosen to provide the desired

saturation kinetic profiles (e.g., sigmoidal kinetics, [P2] > [P1], etc.). For simulation of saturation

curves, initial substrate concentrations were varied between 0 and 300 μM, $E_t$ was 5 nM and the

incubation time were set at 5, 10, or 20 min. Substrate consumption in all saturation curve

simulations was <10% unless indicated. $CL_{int}$ was simulated as d[S]/dt / [S], over a range of 0.01

– 1 μM initial substrate concentrations, with $E_t$ =100 nM. Triplicate data with random error of

substrate concentrations and incubation time were simulated from ESSP and ESSP1P2 ODEs,

respectively. For some simulations and parameterizations, correlation between parameters is

expected, and some parameters must be held constant. For example, if an enzyme species is not

saturated within the range of substrate concentrations, both $k_{cat}$ and $K_m$ cannot be determined.

One parameter must be held constant and only the ratio of $k_{cat}/K_m$ can be determined.

Simulated datasets were generated via the built-in function NDSolve in Mathematica 12.0

(Wolfram Research, Champaign, IL). Random errors were generated from RandomVariate and

NormalDistribution function by setting the mean as one and relative standard deviation as 1%,

5%, 10%, and 20%. This error was multiplied by the simulated values to generate log-normally

distributed values. For the simulations, 500 runs of triplicate data were generated at each error

level.

**Model fitting.** For the derived velocity equation method, the Michaelis-Menten equation and

ESSP rate equation (Eq. 2) were fit to the simulated concentration-velocity data. The

NonlinearModelFit function was used to parameterize the model with 1/Y weighting.

$$\frac{velocity\ (v)}{E_t} = \frac{k_{cat1}\ S + \frac{k_{cat2}}{K_{m2}}\ S^2}{K_{m1} + S + \frac{S^2}{K_{m2}}}\ (2)$$

DMD-AR-2021-000553R1

For numerical analyses, each metabolite concentration dataset (triplicate) was used to

parameterize the micro rate constants of the ESP and ESSP ODEs using NDSolve (MaxSteps →

10,0000 and PrecisionGoal → ∞) and NonlinearModelFit with 1/Y weighting. Two metabolite

concentration datasets (triplicate) were used to simultaneously parameterize the micro rate

constants of the ESP1P2 and ESSP1P2 ODEs.

13

DMD-AR-2021-000553R1

**Results**

**Two-substrate binding and single product formation**. Two substrate binding can lead to

atypical saturation kinetic behavior (biphasic, substrate inhibition and sigmoidal). Sigmoidal

kinetics can be observed for two general scenarios: $K_{m2} < K_{m1}$ and/or $k_{cat2} > k_{cat1}$. These general

cases and the specific cases when $k_{cat1} = 0$ are listed in Table 1 and simulations are shown in Fig.

3. Fig. 3 shows simulations for four possible scenarios of sigmoidal kinetics. All of the plots in

Fig. 3 show sigmoidal saturation. The impact of relative differences in kinetic parameters on the

degree of sigmoidicity is also shown. When $k_3 > 0$, a linear range is observed at low

concentrations (Figs. 3B and 3C). When $k_3 = 0$, no linear range is observed (Figs. 3C and 3D).

The implication of not having a linear range is significant. In the field of drug metabolism, a

linear $V_{max}/K_m$ describes a constant in vitro intrinsic clearance. Fig. 4 shows the concentration-

dependence of $CL_{int}$ for the sigmoidal kinetic curves in Fig. 3. In Cases I and II, at most a 2-fold

difference in $CL_{int}$ would be observed at concentrations < 1 μM. It is noteworthy that up to a

100-fold difference in $CL_{int}$ may be observed in Cases III and IV.

**Two-substrate binding and two product formation.** Although CYPs can usually form multiple

metabolites, most of the kinetic models for atypical kinetics consider the dominant metabolite.

Although some CYPs can form more then two primary metabolites, for simplicity we have

simulated the formation of two metabolites from the same CYP. The scheme in Fig. 5A assumes

that the formation steps for both products are rate-limiting and P1 shows sigmoidal kinetics (Fig.

5B) since ESS formation has a higher velocity for P1 formation. Although P2 appears to have an

almost hyperbolic saturation curve (Fig. 5C), the Eadie Hofstee (EH) plot shows the kinetics are

atypical. This is because there is some minimal sigmoidicity due to ESS formation, even when

14

the apparent $K_m$ and $k_{cat}$ for ES and ESS values are identical.  Similar to Fig. 4, the higher the

$k_7/k_3$ ratio, the greater the change in P1 formation $CL_{int}$ with increasing [S]. P2 formation $CL_{int}$ is

constant when varying $k_7$, since substrate oxidation is not rate-limiting.


The scheme in Fig. 6A assumes that formation of active oxygenating species is rate-limiting.

Again, P1 shows sigmoidal kinetics (Fig. 6B), but P2 now shows substrate inhibition (Fig. 6C).

Substrate inhibition increases for P2 with increased $k_7/k_3$ ratio.


The probability distribution of parameters to compare the use of single versus multiple substrate

models, velocity equations versus ODEs, and single versus multiple product formation is shown

in Fig. 7. These simulations (n = 500) were performed using a multiple substrate, multiple

product scheme (ESSP1P2) at error levels of 1%, 5% and 10%. In all cases, ESS models were

necessary to accurately parameterize $K_{m1}$ and $k_{cat1}$. Although the means were approximately the

same for all ESS models, the distribution was narrowest for the ESS models when both products

were modeled simultaneously. Parameters for all models tested are listed in Supplementary

Table S1.


**Sequential metabolism.** CYPs can also metabolize substrates in sequentially to multiple

metabolites. In this section we simulated sequential metabolism using single-substrate (Fig. 8)

and two-substrate binding kinetic models (Fig. 9). The kinetic scheme in Fig. 8A includes the

EP1 intermediate. If P2 formation from P1 is slower than the P1 release rate, P2 will show a lag

time since accumulation and rebinding of P1 to the CYP active site is necessary for P2 formation

(Fig. 8B).  If P2 formation from P1 is much faster than the P1 release rate, P2 will not show a lag

15

time. Assuming linear product formation for P1, the velocities measured at different incubation time yields the same saturation curves for P1 but not with P2 (Fig. 8C).

Fig. 8D shows the relationship of the rate of P1 release ($k_5$) and the sequential metabolism turnover ($k_6$). At $k_6 = 27$ min$^{-1}$, varying the ratio of $k_5/k_6$ from 100 to 1 results in P1 dissociation constants from 10 to 0.1 $\mu$M. Increasing the rate of P2 formation leads to a decrease in P1 formation and an increase in P2. Substrate inhibition for P2 formation becomes apparent in the Eadie-Hofstee plot since substrate competes for free enzyme with the rebinding of P1.

Sequential metabolism was also simulated with a two-substrate binding kinetic model (Fig. 9A). However, this model assumes P1 release is fast and must compete with substrate binding for free enzyme. Provided that P1 release is faster than P2 formation, these simulations should be relevant. Three types of ESS formation were simulated: when $k_3 = k_6$, $k_3 > k_6$ and at $k_3 < k_6$ (Figs. 9B-D, respectively). An increase in P1 affinity led to a decrease in velocity of P1 and increase in the formation of P2. As expected, P1 formation shows slight sigmoidal, substrate inhibition, and sigmoidal kinetics for $k_3 = k_6$, $k_3 > k_6$ and at $k_3 < k_6$, respectively. The saturation curve for P2 follows that for P1 at low [S]. At high [S], P2 formation shows substrate inhibition for all cases since increasing substrate concentrations competes with P1 rebinding.

Using numerical methods, any of the above approaches to model multi-product and sequential metabolism can be combined. Fig. 10A shows a scheme where two products (P1 and P2) can be formed from an ESS model, and one of the products is further metabolized to a third product, P3. In Fig. 10B, both initial products can be metabolized to the same secondary product by

16

DMD-AR-2021-000553R1

sequential metabolism. For the simulations in Fig. 10C, the substrate binding constants were held

constant with $k_1$, $k_5$ and $k_9$ =270 $\mu M^{-1}$ $min^{-1}$, $k_2$ and $k_6$ = 10000 $min^{-1}$ (Rittle and Green, 2010),

and the turnover rates for P1 and P2 formation were held constant with $k_3$ = 1 $min^{-1}$, $k_7$ = 100

$min^{-1}$, and $k_4$ = $k_8$ = 1 $min^{-1}$. In these simulations, the dissociation constants for P1 binding were

modeled at 10 and 0.1 $\mu M$. In Fig 10C we can see that as the affinity for P1 to the enzyme

increases, P1 is rapidly converted to P3 and the ratio of P1 to P2 is decreased. As substrate

concentrations are increased, P1 binding is inhibited and the expected change in P1/P2 ratios are

observed. Finally, Fig. 10D shows that both the affinity and rates of sequential metabolism affect

the P1/P2 ratios at different substrate concentrations.

17

**Discussion**

The goals of this manuscript (Part 1) are four-fold: 1) to simulate and evaluate atypical kinetics using both derived velocity equations and numerical solutions using ODEs and compare the results; 2) to evaluate the impact of multiple metabolites on these models; 3) to evaluate the impact of atypical kinetics for reactions that show sequential metabolism; and 4) to provide the theoretical basis for analysis of datasets discussed in Part 2 of these manuscripts. The focus of this manuscript is on schemes and parameters that display sigmoidal saturation kinetics since these results are the most difficult to interpret.

Two standard in vitro experiments to characterize CYP-mediated oxidations are saturation curves and substrate depletion assays. Substrate depletion assays observe the loss of substrate over time, usually in a microsomal incubation. This assay only requires quantitation of the substrate, a simple task since the structure is known. The assay provides an initial estimate of hepatic stability. If first-order elimination is assumed, the elimination rate constant can be used to estimate intrinsic clearance ($CL_{int}$). This clearance value can be scaled up to a human $CL_{int}$ using standard methods (Ito et al., 1998; Chiba et al., 2009). Once metabolites are known and standards are available, saturation curves are used to determine kinetic constants i.e. substrate affinities and velocities. Comparing parameters for different enzymes, one can determine which CYPs form which metabolites and which enzymes are likely to be important clinically. These kinetic parameters can also be used to predict whether a drug will be a victim or perpetrator of drug interactions.

18

Non-Michaelis-Menten kinetics are often observed for CYP-mediated oxidation reactions,

resulting in non-hyperbolic saturation curves, for example, sigmoidal saturation, substrate

inhibition, and biphasic saturation curves (Korzekwa et al., 1998). These saturation curves are a

result of multiple substrates binding simultaneously to the enzyme (e.g. Fig. 1B). Most CYP-

catalyzed reactions saturate well above unbound therapeutic concentrations. This results in linear

pharmacokinetics since drug elimination occurs in the linear portion of the saturation curve. For

substrate inhibition and biphasic saturation curves, the saturation curve is approximately linear

below the $K_m$ for ES formation. This is because the binding of the first substrate (higher affinity

binding) still has a linear region at low substrate concentrations. Substrate inhibition and biphasic

saturation would have to occur at very low substrate concentrations to be clinically relevant. On

the other hand, sigmoidal saturation curves can be more problematic. Sigmoidal kinetics can

occur when either ESS formation occurs with a higher affinity than ES formation or if $k_{cat2}$ from

ESS is faster than $k_{cat1}$ from ES (e.g. $k_6 > k_3$ in Fig. 1B). If $k_{cat1}$ contributes substantially at

therapeutic concentrations, there may still be a linear region. However, if $k_{cat1}$ approaches zero,

there may not be a linear region at low substrate concentrations. This will result in a different

estimate of intrinsic clearance for different initial substrate concentrations (e.g. see Fig. 4). An

example of the impact of using an Michaelis-Menten model to predict the intrinsic clearance of

an enzyme showing sigmoidal kinetics is shown in Part 2 of these manuscripts.

The results in Fig. 3 are as expected, with the sigmoidal saturation curves having a linear region

at low substrate concentrations when $k_{cat1}$ ($k_3$) is $> 0$ (Figs. 3B and C) and no linear region when

$k_3 = 0$ (Figs. 3D and E). All simulations give the expected Eadie-Hofstee plots showing convex

curvature to the right. Fig. 4 shows the impact of low $k_{cat1}$ values on $CL_{int}$. When $k_{cat1}$ is 1,

sigmoidicity due to either higher affinity binding of the second substrate or higher velocity of the

second substrate results in modest increases in $CL_{int}$ (~2 fold between 10 nM and 1 μM for 100-

fold increases in affinity or velocity for ESS; Figs. 4A and B). However, when $k_{cat1} = 0$, ~ 100-

fold increases in $CL_{int}$ are observed for [S] between 10 nM and 1 μM (Figs. 4C and D). Also,

there is no range where $CL_{int}$ is constant. An ~ 100-fold increase in $CL_{int}$ would be observed for

[S] between 0.1 nM and 10 nM as well. This nonlinearity can be identified with substrate

depletion assays at different substrate concentrations. Predicting in vivo $CL_{int}$ would require

conducting in vitro assays at [S] that match the unbound intracellular concentrations. Also,

concentration-dependent $CL_{int}$ in vitro may result in non-linear pharmacokinetics in vivo.


Sequential metabolism by the CYPs is important in drug discovery and development, since

metabolites can be active, toxic, or cause drug-drug interactions (Jackson et al., 2018; Wienkers

and Rock, 2021)  We have simulated CYP kinetic models that can form two different products

from either a single substrate complex (Figs. 2A and C) or from an ESS complex (Figs. 2B and

D).  These models do not include both multiple product formation and sequential metabolism.  If

a substrate can only bind once (Figs. 2A and C) the P1/P2 product ratio remains constant at $k_3/k_4$.

However, for multi-substrate kinetics, metabolite ratios can change with substrate

concentrations. Fig. 5 is the simplest scheme for two products formed from ES and ESS

complexes. The simulations in Fig. 5 shows increasing formation of P1 from ESS while holding

all other parameters constant. As expected, P1 formation shows increasing sigmoidicity as $k_7$

increases due to the higher velocity for P1 formation from ESS. However, this scheme does not

accurately capture the impact of increasing one product formation pathway for a CYP reaction.

As shown in Fig. 5C, changing $k_7$ has no impact on P2 formation. This is because binding is fast

and the rate-limiting steps in this scheme are the product formation steps ($k_3$, $k_4$, $k_7$, and $k_8$). In

reality, the rate-limiting step for CYP oxidations is the formation of an active oxygenating

species, and this active oxygenating species can form different metabolites. This results in the

CYP property called "metabolic switching" where blocking one site results in increased

metabolism at other sites. This can be best modeled using the schemes in Figs. 2C and D and

Fig. 6.  In Fig. 6C, increasing $k_7$ while holding all parameters constant results in a decrease in P2

formation at high substrate concentrations. Since formation of the active oxygenating species is

rate-limiting, increasing P1 formation must result in a decrease in P2 formation. For a chemist

modifying a molecule for stability, the difference between the schemes in Figs. 5 and 6 is

important, since decreasing metabolism at one position may increase metabolism at another.

However, when fitting kinetic models to experimental datasets for multiple products, the simpler

scheme in Fig. 5 is preferred. The same substrate inhibition profile for P2 seen in Fig. 6C would

also be observed if $k_8 < k_4$. Using the method of Cleland (Cleland, 1975) and the scheme in Fig.

6, net rate constants can be calculated for conversion of ES and ESS complexes to products, and

the result is the simplified scheme in Fig. 5. For example, the net rate constant for P1 formation

from ES in Fig. 6 ($k_{a1}$ $k_3/(k_3+k_4)$) will be equal to $k_3$ in Fig. 5.


The parameter probability distributions for the various simulations shown in Fig. 7 shows that 1)

using an ES model for ESS kinetics results in inaccurate $K_m$ and $k_{cat}$ values; 2) use of ODEs

instead of derived velocity equations minimizes the overall parameter errors; and 3)

simultaneous fitting to both P1 and P2 data further decreases the parameter errors. These results

suggest that using ODEs to model CYP kinetics is generally preferred to using derived velocity

21

equations. Derived velocity equations include additional simplifying assumptions, and equations

for complex systems these equations are generally not available.

When sequential metabolism occurs, the rate of the first product release (P1 in Fig. 8A) has a

large impact on the kinetics of the sequential product (P2). If P1 release is fast, there will be a lag

time for P2 formation, since P1 must accumulate before P2 can be formed. Also, P2 formation

can be inhibited by high substrate concentrations. Lag times have frequently been observed for

time-dependent inhibition kinetics when multiple oxidation steps are required for CYP

inactivation. Fig. 9 considers a scenario including multiple substrate binding and sequential

metabolism with mandatory P1 release. A complete model would additionally include ESP1,

ESP2, EP1P1, EP1P2 and EP2P2. Limiting schemes to mandatory product release may not

always be sufficient to model experimental data (see Part 2). Finally, schemes can be readily

constructed for multiple substrate binding with multiple product formation as well sequential

metabolism (Fig. 10). Adding sequential metabolism can result in unusual P1/P2 product ratio

curves when one or both products are further metabolized. A wide range of product ratio curves

is possible for a variety of schemes and kinetic scenarios (e.g. see Fig. 10D). When experimental

data are available for both P1 and P2 formation, product ratio plots can be very useful in

selecting appropriate kinetic schemes (see Part 2).

Mechanisms can vary for different substrates with the same CYP, and for different CYPs with

the same substrate. The diversity of possible mechanisms requires that statistical methods be

used to determine the best model for a given dataset. We use AICc values to compare different

mechanisms since this method can be used for nested and non-nested models. It is also important

to plot residuals. A run of signs indicates that the model is likely inadequate and may bias data interpretation. Parameter errors should be compared to the parameter estimates, since covariance will result in large relative parameter errors. This can also be observed in the correlation matrix for the calculation. It should be noted that insufficient data and high experimental errors can result in inaccurate model selection.

Finally, in Part 2 of these manuscripts, we have used numerical methods to simultaneously model the multiple metabolites formed initially and sequentially from diazepam by CYP3A4. This resulted in a mechanistic interpretation of diazepam metabolism that provided affinities and velocities consistent with the observed metabolic data for diazepam and its metabolites.

In conclusion, we have modeled combinations of multiple substrate binding, multiple product formation and sequential metabolism. We have focused on sigmoidal kinetics since it can have a dramatic impact on clearance predictions. The use of Michaelis-Menten models to characterize multi-substrate saturation data results in inaccurate kinetic parameters and clearance predictions. Comparing results for use of standard velocity equations with ODEs clearly shows that ODEs are more versatile and provide better parameter estimates. The complexity of the kinetic schemes used for these analyses shows that most kinetic schemes can be modeled, and these models can be parameterized, provided that sufficient experimental data is available. Finally, these analyses provide a framework for modeling the experimental CYP kinetics observed in Part 2 of these manuscripts.

DMD-AR-2021-000553R1

## Authorship Contributions

*Participated in research design:* Wang Z, Paragas EM, Korzekwa K

*Conducted experiments:* Wang Z, Paragas EM

*Performed data analysis:* Wang Z, Paragas EM, Nagar S, Korzekwa K

*Wrote or contributed to the writing of the manuscript:* Wang Z, Paragas EM, Nagar S, Korzekwa

K

24

**References**

Atkins WM (2005) Non-Michaelis-Menten kinetics in cytochrome P450-catalyzed reactions. *Annu Rev Pharmacol Toxicol* **45:**291-310.

Atkins WM (2006) Current views on the fundamental mechanisms of cytochrome P450 allosterism. *Expert Opin Drug Met* **2:**573-579.

Barnaba C, Yadav J, Nagar S, Korzekwa K, and Jones JP (2016) Mechanism-based inhibition of CYP3A4 by podophyllotoxin: aging of an intermediate is important for in vitro/in vivo correlations. *Mol Pharm* **13:**2833-2843.

Blobaum AL, Bridges TM, Byers FW, Turlington ML, Mattmann ME, Morrison RD, Mackie C, Lavreysen H, Bartolomé JM, Macdonald GJ, Steckler T, Jones CK, Niswender CM, Conn PJ, Lindsley CW, Stauffer SR, and Daniels JS (2013) Heterotropic Activation of the Midazolam Hydroxylase Activity of CYP3A by a Positive Allosteric Modulator of mGlu5: In Vitro to In Vivo Translation and Potential Impact on Clinically Relevant Drug-Drug Interactions. *Drug Metabolism and Disposition* **41:**2066-2075.

Chiba M, Ishii Y, and Sugiyama Y (2009) Prediction of hepatic clearance in human from in vitro data for successful drug development. *AAPS J* **11:**262.

Cleland WW (1975) Partition analysis and the concept of net rate constants as tools in enzyme kinetics. *Biochemistry* **14:**3220-3224.

Cleland WW (1979) Statistical analysis of enzyme kinetic data. *Methods Enzymol* **63**.

Collom SL, Laddusaw RM, Burch AM, Kuzmic P, Perry MD, Jr., and Miller GP (2008) CYP2E1 substrate inhibition. Mechanistic interpretation through an effector site for monocyclic compounds. *J Biol Chem* **283:**3487-3496.

Dangi B, Davydova NY, Maldonado MA, Ahire D, Prasad B, and Davydov DR (2021) Probing functional interactions between cytochromes P450 with principal component analysis of substrate saturation profiles and targeted proteomics. *Arch Biochem Biophys* **708:**108937.

Davydov DR, Davydova NY, Rodgers JT, Rushmore TH, and Jones JP (2017) Toward a systems approach to the human cytochrome P450 ensemble: interactions between CYP2D6 and CYP2E1 and their functional consequences. *Biochem J* **474:**3523-3542.

Domanski TL, He YA, Khan KK, Roussel F, Wang QM, and Halpert JR (2001) Phenylalanine and tryptophan scanning mutagenesis of CYP3A4 substrate recognition site residues and effect on substrate oxidation and cooperativity. *Biochemistry* **40:**10150-10160.

Ekins S, Stresser DM, and Williams JA (2003) In vitro and pharmacophore insights into CYP3A enzymes. *Trends Pharmacol Sci* **24:**161-166.

Ekroos M and Sjögren T (2006) Structural basis for ligand promiscuity in cytochrome P450 3A4. *Proc Nat Acad Sci* **103:**13682.

Frenzen CL and Maini PK (1988) Enzyme kinetics for a two-step enzymic reaction with comparable initial enzyme-substrate ratios. *Journal of Mathematical Biology* **26:**689-703.

Galetin A, Brown C, Hallifax D, Ito K, and Houston JB (2004) Utility of recombinant enzyme kinetics in prediction of human clearance: Impact of variability, CYP3A5, and CYP2C19 on CYP3A4 probe substrates. *Drug Metab Dispos* **32:**1411-1420.

Galetin A, Clarke SE, and Houston JB (2003) Multisite kinetic analysis of interactions between prototypical CYP3A4 subgroup substrates: midazolam, testosterone, and nifedipine. *Drug Metab Dispos* **31:**1108-1116.

DMD-AR-2021-000553R1

Gay SC, Roberts AG, and Halpert JR (2010) Structural features of cytochromes P450 and ligands that affect drug metabolism as revealed by x-ray crystallography and NMR. *Future Med Chem* **2:**1451-1468.

Guengerich FP (2018) Mechanisms of cytochrome P450-catalyzed oxidations. *ACS Catal* **8:**10964-10976.

Hemker P (1972) Numerical methods for differential equations in system simulation and in parameter estimation. *Analysis and Simulation of biochemical systems* **28:**59-80.

Hosea NA, Miller GP, and Guengerich FP (2000) Elucidation of distinct ligand binding sites for cytochrome P450 3A4. *Biochemistry* **39:**5929-5939.

Hutzler JM and Tracy TS (2002) Atypical kinetic profiles in drug metabolism reactions. *Drug Metab Dispos* **30:**355-362.

Ito K, Iwatsubo T, Kanamitsu S, Nakajima Y, and Sugiyama Y (1998) Quantitative prediction of in vivo drug clearance and drug interactions from in vitro data on metabolism, together with binding and transport. *Annu Rev Pharmacol Toxicol* **38:**461-499.

Iwaki M, Niwa T, Tanaka H, Kawase A, and Komura H (2019) Prediction of hepatic clearance of stereoselective metabolism of carvedilol in liver microsomes and hepatocytes of Sprague-Dawley and cytochrome P450 2D-deficient dark Agouti rats. *J Pharm Pharm Sci* **22:**72-84.

Jackson K, Durandis R, and Vergne M (2018) Role of Cytochrome P450 Enzymes in the Metabolic Activation of Tyrosine Kinase Inhibitors. *International Journal of Molecular Sciences* **19:**2367.

Jamakhandi AP, Kuzmic P, Sanders DE, and Miller GP (2007) Global analysis of protein-protein interactions reveals multiple CYP2E1-reductase complexes. *Biochemistry* **46:**10192-10201.

Johnson KA (2009) Chapter 23 Fitting Enzyme Kinetic Data with KinTek Global Kinetic Explorer, pp 601-626, Elsevier.

Jones JP and Korzekwa KR (1996) Predicting the rates and regioselectivity of reactions mediated by the P450 superfamily. *Method Enzymol* **272:**326-335.

Kenworthy KE, Clarke SE, Andrews J, and Houston JB (2001) Multisite kinetic models for CYP3A4: simultaneous activation and inhibition of diazepam and testosterone metabolism. *Drug Metab Dispos* **29:**1644-1651.

Komura H, Kawase A, and Iwaki M (2005) Application of substrate depletion assay for early prediction of nonlinear pharmacokinetics in drug discovery: Assessment of nonlinearity of metoprolol, timolol, and propranolol. *J Pharm Sci* **94:**2656-2666.

Korzekwa K (2021) Enzyme Kinetics of Oxidative Metabolism-Cytochromes P450. *Methods Mol Biol* **2342:**237-256.

Korzekwa K, Tweedie D, Argikar UA, Whitcher-Johnstone A, Bell L, Bickford S, and Nagar S (2014) A numerical method for analysis of in vitro time-dependent inhibition data. Part 2. Application to experimental data. *Drug Metab Dispos* **42:**1587-1595.

Korzekwa KR, Krishnamachary N, Shou M, Ogai A, Parise RA, Rettie AE, Gonzalez FJ, and Tracy TS (1998) Evaluation of atypical cytochrome P450 kinetics with two-substrate models: evidence that multiple substrates can simultaneously bind to cytochrome P450 active sites. *Biochemistry* **37:**4137-4147.

Kuzmič P (2009) DynaFit—A Software Package for Enzymology, pp 247-280.

Li H and Poulos TL (2004) Crystallization of cytochromes P450 and substrate-enzyme interactions. *Curr Top Med Chem* **4:**1789-1802.

Luthra A, Denisov IG, and Sligar SG (2011) Spectroscopic features of cytochrome P450 reaction intermediates. *Arch Biochem Biophys* **507:**26-35.

Manimozhi P, Subbiah A, and Rajendran L (2010) Solution of steady-state substrate concentration in the action of biosensor response at mixed enzyme kinetics. *Sensors and Actuators B: Chemical* **147:**290-297.

Masubuchi Y, Iwasa T, Fujita S, Suzuki T, Horie T, and Narimatsu S (1996) Regioselectivity and substrate concentration-dependency of involvement of the CYP2D subfamily in oxidative metabolism of amitriptyline and nortriptyline in rat liver microsomes. *J Pharm Pharmacol* **48:**925-929.

Michaelis L and Menten ML (1913) Die kinetik der invertinwirkung. *Biochem Z* **49:**352.

Nagar S, Jones JP, and Korzekwa K (2014) A numerical method for analysis of in vitro time-dependent inhibition data. Part 1. Theoretical considerations. *Drug Metab Dispos* **42:**1575-1586.

Nguyen HQ, Kimoto E, Callegari E, and Obach RS (2016) Mechanistic modeling to predict midazolam metabolite exposure from in vitro data. *Drug Metab Dispos* **44:**781.

Obach RS (2013) Pharmacologically active drug metabolites: Impact on drug discovery and pharmacotherapy. *Pharmacol Rev* **65:**578-640.

Pang KS (1995) Kinetics of sequential metabolism - Contribution of parallel, primary metabolic pathways to the formation of a common, secondary metabolite. *Drug Metab Dispos* **23:**166-177.

DMD-AR-2021-000553R1

Plant RE (1979) The efficient numerical solution of biological simulation problems. *Computer Programs in Biomedicine* **10:**1-15.

Rajendran L, Devi MC, Fernandez C, and Peng Q (2018) Mathematical Modeling and Simulation of Nonlinear Process in Enzyme Kinetics, InTech.

Rittle J and Green MT (2010) Cytochrome P450 Compound I: Capture, Characterization, and C-H Bond Activation Kinetics. *Science* **330:**933-937.

Roberts AG, Yang J, Halpert JR, Nelson SD, Thummel KT, and Atkins WM (2011) The structural basis for homotropic and heterotropic cooperativity of midazolam metabolism by human cytochrome P450 3A4. *Biochemistry* **50:**10804-10818.

Schadt S, Bister B, Chowdhury SK, Funk C, Hop CECA, Humphreys WG, Igarashi F, James AD, Kagan M, Khojasteh SC, Nedderman ANR, Prakash C, Runge F, Scheible H, Spracklin DK, Swart P, Tse S, Yuan J, and Obach RS (2018) A decade in the MIST: Learnings from investigations of frug metabolites in drug development under the "Metabolites in Safety Testing" regulatory guidance. *Drug Metab Dispos* **46:**865-878.

Sevrioukova IF and Poulos TL (2017) Structural basis for regiospecific midazolam oxidation by human cytochrome P450 3A4. *Proc Nat Acad Sci* **114:**486.

Shou M, Grogan J, Mancewicz JA, Krausz KW, Gonzalez FJ, Gelboin HV, and Korzekwa KR (1994) Activation of CYP3A4 - Evidence for the simultaneous binding of 2 substrates in a cytochrome-P450 active-site. *Biochemistry* **33:**6450-6455.

Tracy TS (2006) Atypical cytochrome p450 kinetics: implications for drug discovery. *Drugs R D* **7:**349-363.

Ueng Y-F, Kuwabara T, Chun Y-J, and Guengerich FP (1997) Cooperativity in oxidations catalyzed by cytochrome P450 3A4. *Biochemistry* **36:**370-381.

Varón R, Havsteen BH, Valero E, Molina-Alarcón M, García-Cánovas F, and García-Moreno M (2005) Kinetic analysis of the transient phase and steady state of open multicyclic enzyme cascades. *Acta Biochim Pol* **52:**765-780.

Walsky RL and Obach RS (2004) Validated assays for human cytochrome P450 activities. *Drug Metab Dispos* **32:**647-660.

Wester MR, Yano JK, Schoch GA, Yang C, Griffin KJ, Stout CD, Johnson EF, White CR, and Seymour RS (2005) The structure of human cytochrome P4502C9 complexed with flurbiprofen at 2.0-angstrom resolution Allometric scaling of mammalian metabolism. *J Exp Biol* **208:**35630-35637.

Wienkers LC and Rock BM (2021) Multienzyme Kinetics and Sequential Metabolism. *Methods Mol Biol* **2342:**89-112.

Yadav J, Korzekwa K, and Nagar S (2018) Improved predictions of drug-drug interactions mediated by time-dependent inhibition of CYP3A. *Mol Pharm* **15:**1979-1995.

Yadav J, Korzekwa K, and Nagar S (2021) Numerical Methods for Modeling Enzyme Kinetics. *Methods Mol Biol* **2342:**147-168.

Yadav J, Paragas E, Korzekwa K, and Nagar S (2020) Time-dependent enzyme inactivation: Numerical analyses of in vitro data and prediction of drug-drug interactions. *Pharmacol Ther* **206**.

Yano JK, Wester MR, Schoch GA, Griffin KJ, Stout CD, and Johnson EF (2004) The structure of human microsomal cytochrome P450 3A4 determined by x-ray crystallography to 2.05-A resolution. *J Biol Chem* **279:**38091-38094.

Yoon MY, Campbell AP, and Atkins WM (2004) "Allosterism" in the elementary steps of the cytochrome P450 reaction cycle. *Drug Metab Rev* **36:**219-230.

Zanger UM and Schwab M (2013) Cytochrome P450 enzymes in drug metabolism: Regulation

of gene expression, enzyme activities, and impact of genetic variation. *Pharmacol Ther*

**138:**103-141.

DMD-AR-2021-000553R1

**Footnotes**

Financial Disclosure and Conflict of Interest: The authors have no financial disclosures, and no

conflicts of interest to report.

**Figure Legends**

Figure 1. Schemes for single product formation. (A) A single-substrate binding (ES complex), one metabolite formation (ESP) scheme is depicted EP complex is not shown since fast product release is assumed. (B) A two-substrate binding (ESS complex), one metabolite formation (ESSP) scheme is depicted. EP, ESP, and EPP are not shown since fast product release and no interaction between substrate and product within the active site are assumed. (C) Expressions for $K_m$ and $k_{cat}$ for schemes A (dashed purple box) and B (dashed blue box) are listed. Rate constants for all reactions are denoted by $k_1$–$k_6$. The species depicted in the schemes are defined as follows: E, unbound enzyme; P1, product 1; ES, enzyme-substrate complex; and ESS, enzyme-substrate-substrate complex.

Figure 2. Schemes for multiple product formation. (A) A single-substrate binding, two metabolite formation (ESP1P2) scheme. (B) A two-substrate binding, two metabolite formation (ESSP1P2) scheme. (C) Single-substrate binding with rate-limiting oxygen activation. (D) multiple-substrate binding with rate-limiting oxygen activation (E) Expressions for $K_m$ and $k_{cat}$ for schemes A (dashed purple box) and B (dashed blue box) are listed. Rate constants for all reactions are denoted by $k_1$–$k_8$. Rate constants $k_{a1}$ and $k_{a2}$ denote oxygen activation steps for ES* and ESS* respectively. The species depicted in the schemes are defined as follows: E, unbound enzyme; P1, product 1; P2, product 2; ES, enzyme-substrate complex; and ESS, enzyme-substrate-substrate complex; ES* and ESS*, active oxygen species.

34

Figure 3. Sigmoidal saturation curves for multiple-substrate binding and single product formation. (A) Enzyme kinetic scheme. (B-E) Top: saturation curves (0-300 μM) with inset Eadie-Hofstee plots; Bottom: saturation curves (0-0.1 μM). Common micro rate constants: $k_1 = k_4 = 270$ μM$^{-1}$min$^{-1}$, $k_2 = 22000$ min$^{-1}$. Other fixed rate constants are shown at the top of each column and varying rate constants are at the bottom. Units for $k_3$, $k_5$, $k_6$ are min$^{-1}$.

Figure 4. Concentration dependence of CL$_{int}$ for the ESS model. (A-D) CL$_{int}$ as a function of [S] for scenarios in Table 1 and Fig. 3. The arrows indicate the fold changes in CL$_{int}$ at 0.01, 0.1 and 1 μM. Common micro rate constants: $k_1 = k_4 = 270$ μM$^{-1}$min$^{-1}$, $k_2 = 22000$ min$^{-1}$. Units for $k_3$, $k_5$, $k_6$ are min$^{-1}$. Note the different scales of the Y-axes.

Figure 5. Saturation curves for multiple-substrate binding and multiple product formation. The scheme assumes that oxygen activation is not rate-limiting. (A) Enzyme kinetic scheme. (B-C) Top: saturation curves for P1 and P2 respectively (0-300 μM) with inset Eadie-Hofstee plots; Bottom: saturation curves for P1 and P2 respectively (0-0.1 μM). (D): [P1]/[P2] metabolite ratio versus [S], with inset at low [S]. The dashed lines represent the $k_3/k_4$ and $k_7/k_8$ ratios. Fixed micro rate constants: $k_1 = k_5 = 270$ μM$^{-1}$min$^{-1}$, $k_2 = k_6 = 10000$ min$^{-1}$, $k_3 = k_4 = k_8 = 1$ min$^{-1}$.

Figure 6. Saturation curves for multiple-substrate binding and multiple product formation. The scheme assumes that oxygen activation is rate-limiting. (A) Enzyme kinetic scheme. (B-C) Top: saturation curves for P1 and P2 respectively (0-300 μM) with inset Eadie-Hofstee plots; Bottom: saturation curves for P1 and P2 respectively (0-0.1 μM). (D): [P1]/[P2] metabolite ratio versus [S], with inset at low [S]. The dashed lines represent the $k_3/k_4$ and $k_7/k_8$ ratios. Fixed micro rate

constants: $k_1 = k_5 = 270$ $\mu M^{-1} min^{-1}$, $k_2 = k_6 = 10000$ $min^{-1}$, $k_3 = k_4 = k_8 = 1000000$ $min^{-1}$, $k_{a1} = k_{a2}$ $= 30$ $min^{-1}$.

Figure 7. The probability distribution of $K_{m1}$, $K_{m2}$, $k_{cat1}$, and $k_{cat2}$ estimates. (A) $K_{m1}$ at 1%, 5% and 10% error. (B) $k_{cat1}$ at 1%, 5% and 10% error. (C) $K_{m2}$ at 1%, 5% and 10% error. (D) $k_{cat2}$ at 1%, 5% and 10% error. The probability distribution for all parameters is depicted for the Michaelis-Menten equation (red), ESS velocity equation (blue), ES ODE (green), ESS ODE (purple), ESP1P2 ODE (orange), and ESSP1P2 ODE (magenta). Distribution is shown for 500 runs at each condition. Data were simulated with the following parameters: $k_1 = k_5 = 270$ $\mu M^{-1}$ $min^{-1}$, $k_2 = 13500$ $min^{-1}$, $k_3 = 1$ $min^{-1}$, $k_4 = 1$ $min^{-1}$, $k_6 = 2700$ $min^{-1}$, $k_7 = 5$ $min^{-1}$, $k_8 = 1$ $min^{-1}$.

Figure 8. Single-substrate binding and sequential metabolism. (A) Enzyme kinetic scheme. (B) P2 concentration over time at $k_5/k_6 = 100$ versus 1, exhibiting a lag time in P2 formation at $k_5/k_6 = 100$. (C) Saturation curve plots for P1 and P2 simulated at different incubation time (t) at the following rate constants: $k_1 = 270$ $\mu M^{-1}$ $min^{-1}$; $k_2 = 2700$ $min^{-1}$; $k_3 = 20$ $min^{-1}$; $k_4 = 270$ $\mu M^{-1}$ $min^{-1}$; $k_5 = 2700$ $min^{-1}$; and $k_6 = 27$ $min^{-1}$. (D) Saturation curve plots for Products 1 and 2 simulated at different rates of product release ($k_5$) and sequential metabolism turnover ($k_6$). Insets: Eadie-Hofstee plots.

Figure 9. Multiple-substrate binding and sequential metabolism. (A) Enzyme kinetic scheme. Saturation curve plots for P1 and P2 simulated at different rates of product dissociation ($k_8$) and sequential metabolism turnover ($k_9$), when (B) $k_3 = k_6 = 27$ $min^{-1}$. (C) $k_3 > k_6$; $k_3 = 100$ $min^{-1}$ and $k_6 = 27$ $min^{-1}$, and (D) $k_3 < k_6$; $k_3 = 27$ $min^{-1}$ and $k_6 = 100$ $min^{-1}$. Fixed values used were: $k_1$, $k_4$

and $k_7 = 270$ $\mu M^{-1}$ $min^{-1}$, $k_2 = 22000$ $min^{-1}$, $k_5 = 11000$ $min^{-1}$, $k_9 = 27$ $min^{-1}$. All insets depict

Eadie-Hofstee plots.

Figure 10. Models for multiple-substrate binding and multiple product formation where (A) one

or (B) two products undergo sequential metabolism. (C) [P1]/[P2] product ratio versus [S] for

model A simulated at increasing sequential turnover rate ($k_{11}$) with $k_{10}$ fixed at 2700 and 27 $min^{-1}$. (D) [P1]/[P2] product ratio versus [S] for model B simulated at increasing sequential turnover

rate of P2 forming P3 ($k_{14}$) with $k_{10}$ fixed at 2700 and 27 $min^{-1}$. Common micro rate constants:

$k_1$, $k_5$, and $k_9 = 270$ $min^{-1}$, $k_2$ and $k_6 = 10000$ $\mu M^{-1}$ $min^{-1}$, $k_3 = 1$ $min^{-1}$ and $k_7 = 100$ $min^{-1}$, $k_4$ and

$k_8 = 1$ $min^{-1}$. For D, $k_{12} = 270$ $min^{-1}$ and $k_{11} = 1$ $min^{-1}$.

**Tables**

Table 1. Different cases for sigmoidal kinetics

| Parameter | Case I | Case II | Case III | Case IV |
|---|---|---|---|---|
| $k_2, k_5$ | $k_2 > k_5$ | $k_2 = k_5$ | $k_2 > k_5$ | $k_2 = k_5$ |
| $(K_{m1}, K_{m2})$ | $(K_{m1} > K_{m2})$ | $(K_{m1} = K_{m2})$ | $(K_{m1} > K_{m2})$ | $(K_{m1} = K_{m2})$ |
| $k_3, k_6$ | $k_6 = k_3$ | $k_6 > k_3$ | $k_6 > k_3 = 0$ | $k_6 > k_3 = 0$ |
| $(k_{cat1}, k_{cat2})$ | $(k_{cat1} = k_{cat2} > 0)$ | $(k_{cat2} > k_{cat1} > 0)$ | $(k_{cat2} > k_{cat1} = 0)$ | $(k_{cat2} > k_{cat1} = 0)$ |

The cases $k_2 > k_5$ ($K_{m1} > K_{m2}$) and $k_6 > k_3 = 0$ ($k_{cat1} > k_{cat2} > 0$) are not discussed.
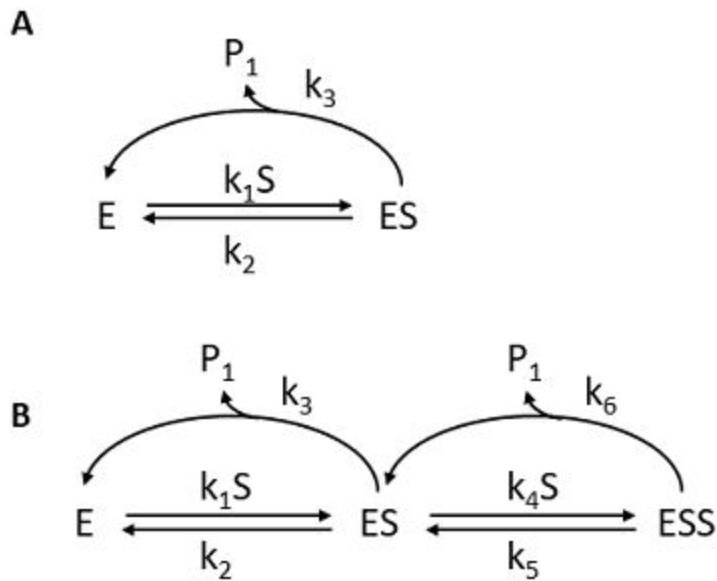
Figure 1.

Figure 2

Figure 3.

**A** — $k_3 = 1$, $k_6 = 1$; Case I; $CL_{int,\,in\,vitro}$, $\mu L\ min^{-1}\ nmol^{-1}$ vs [S], $\mu M$; $k_5/k_2 = $ 0.5, 0.1, 0.05, 0.01 (labels 1, 1.1, 2.1)

**B** — $k_3 = 1$, $k_5 = 22000$; Case II; $CL_{int,\,in\,vitro}$, $\mu L\ min^{-1}\ nmol^{-1}$ vs [S], $\mu M$; $k_6/k_3 = $ 2., 10., 20., 100. (labels 1, 1.1, 1.9)

**C** — $k_3 = 0$, $k_6 = 1$; Case III; $CL_{int,\,in\,vitro}$, $\mu L\ min^{-1}\ nmol^{-1}$ vs [S], $\mu M$; $k_5/k_2 = $ 0.5, 0.1, 0.05, 0.01 (labels 1, 9.9, 90.7)

**D** — $k_3 = 0$, $k_5 = 22000$; Case IV; $CL_{int,\,in\,vitro}$, $\mu L\ min^{-1}\ nmol^{-1}$ vs [S], $\mu M$; $k_6 = $ 0.1, 0.5, 5., 60. (labels 1, 9.9, 94.4)
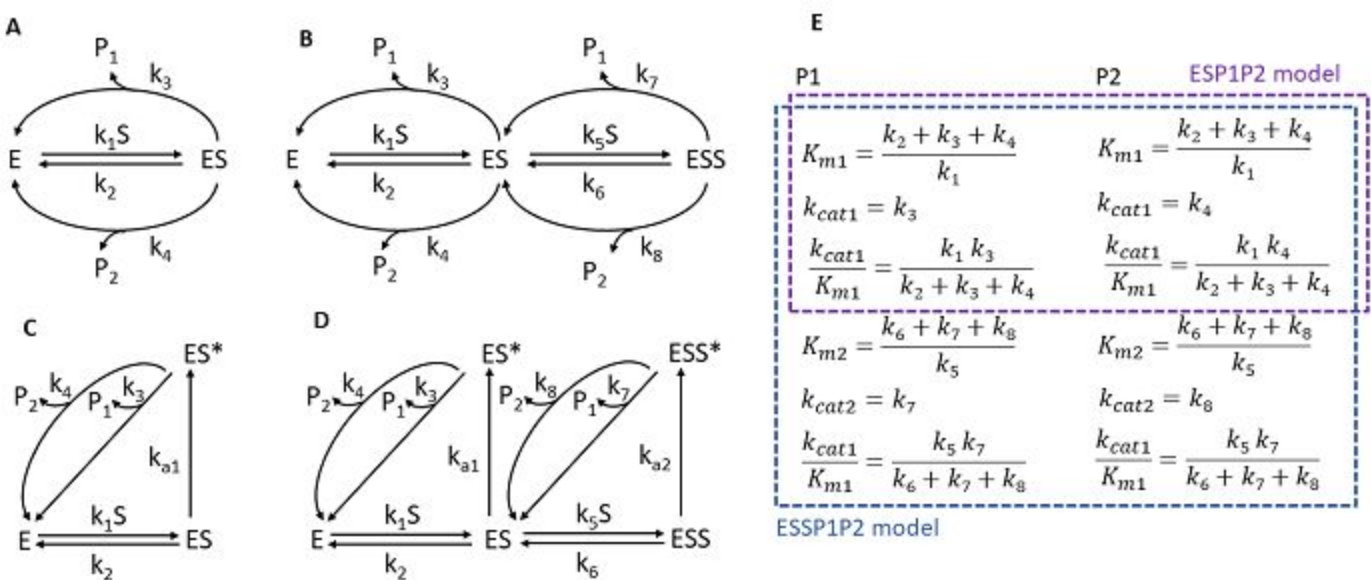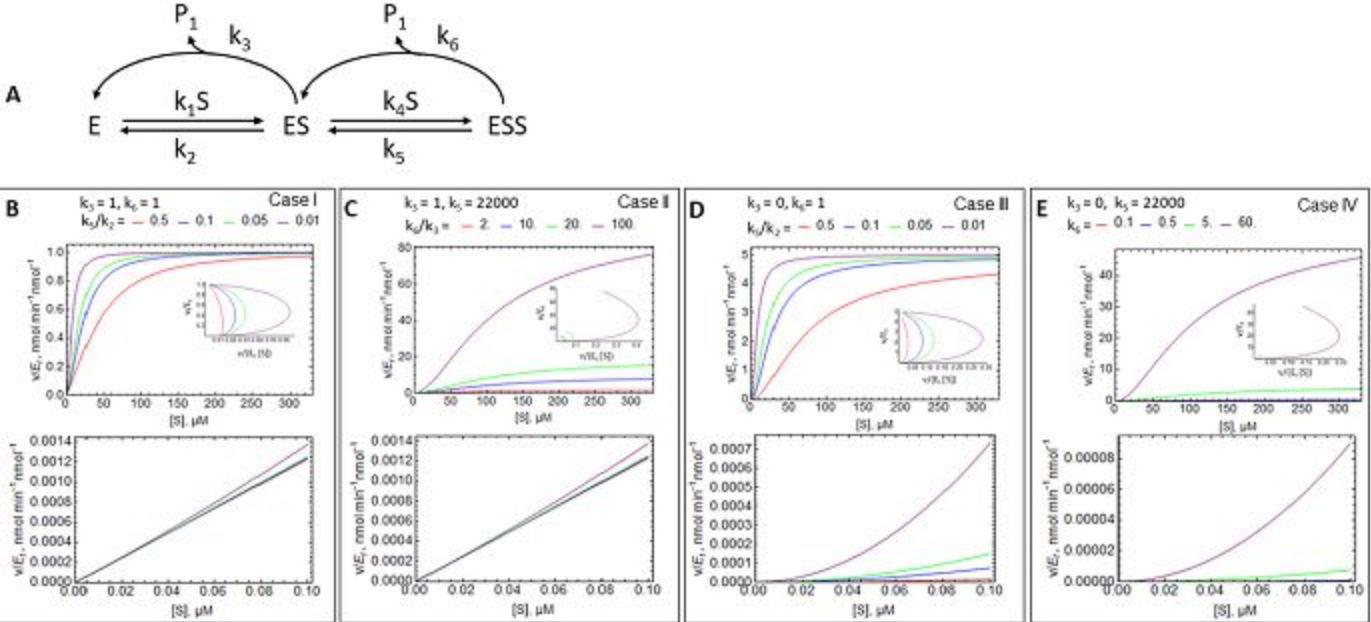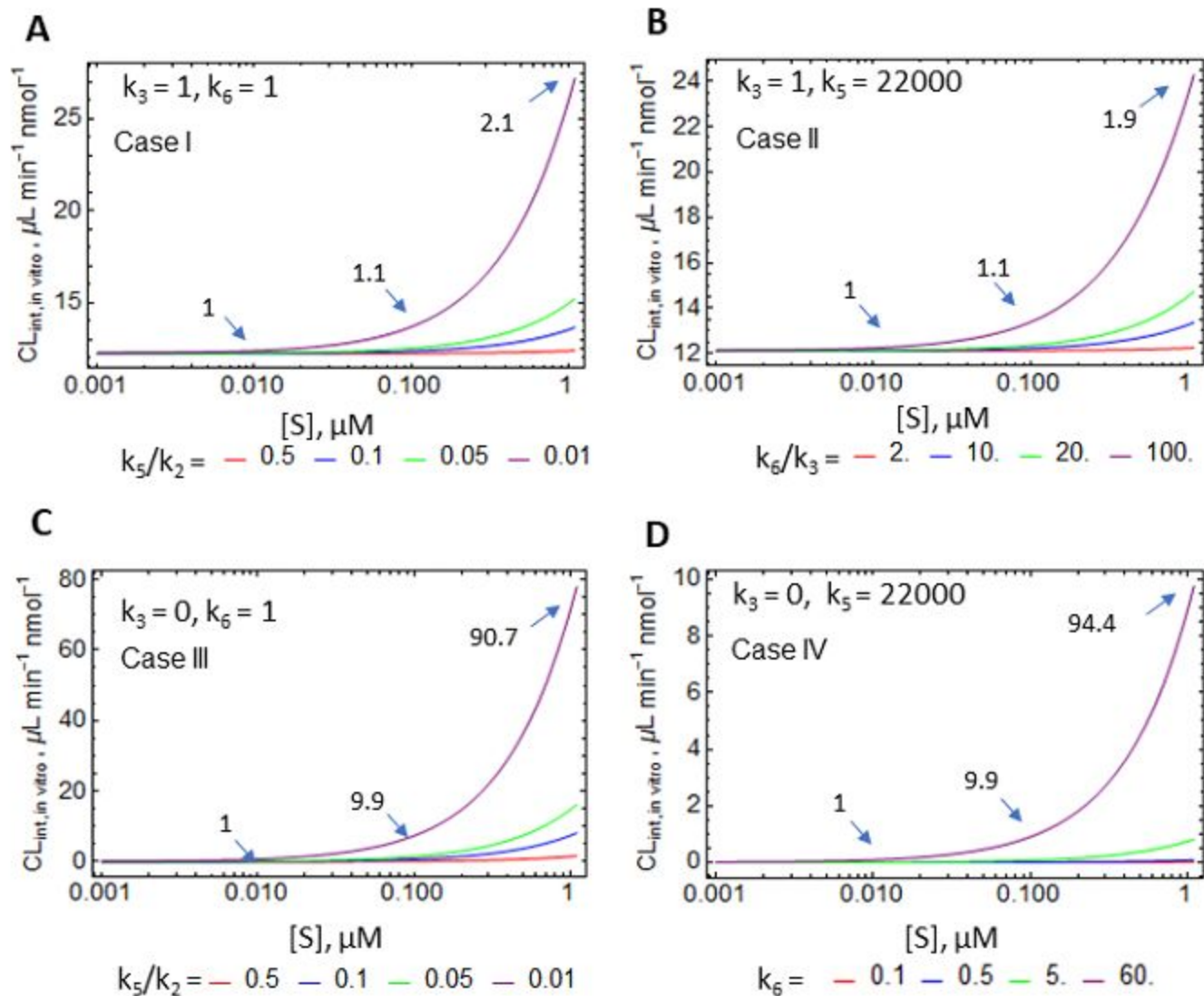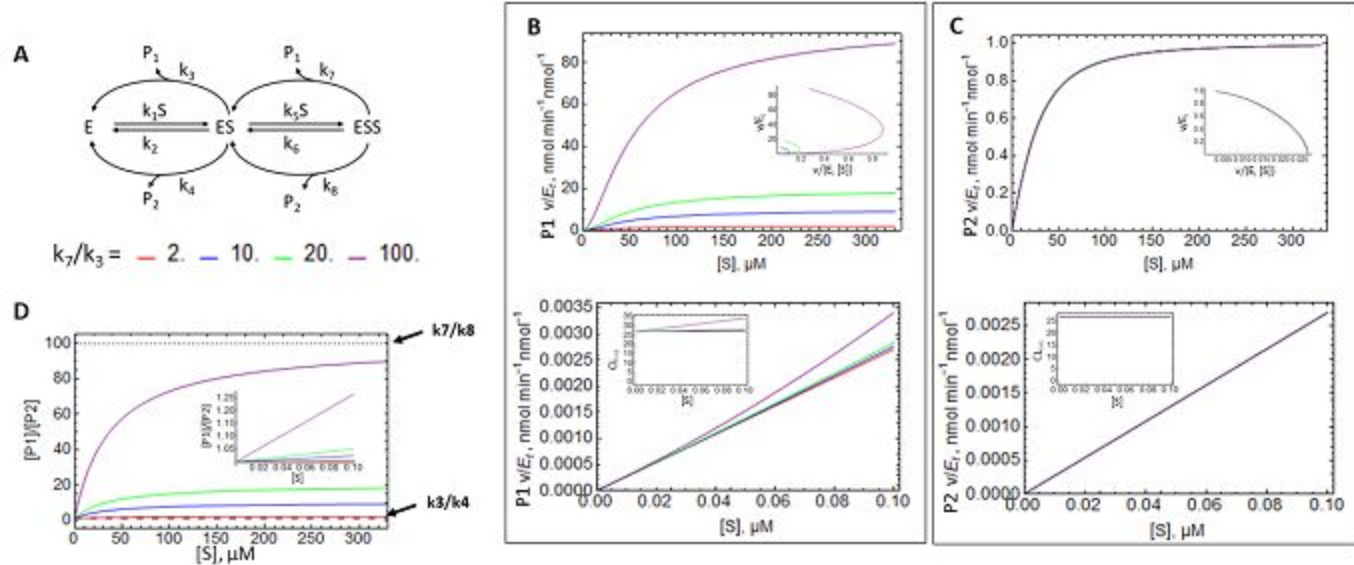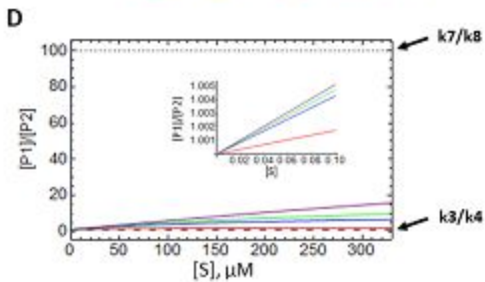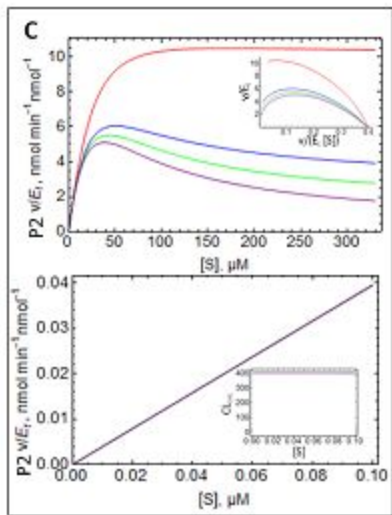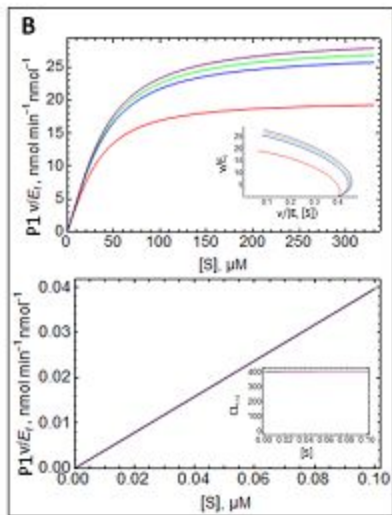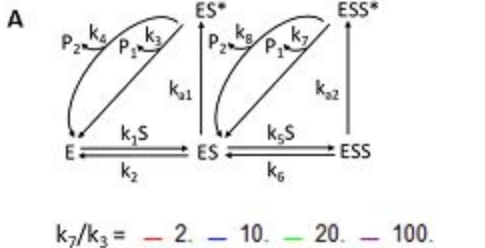
Figure 4.

Figure 5.

Figure 6.
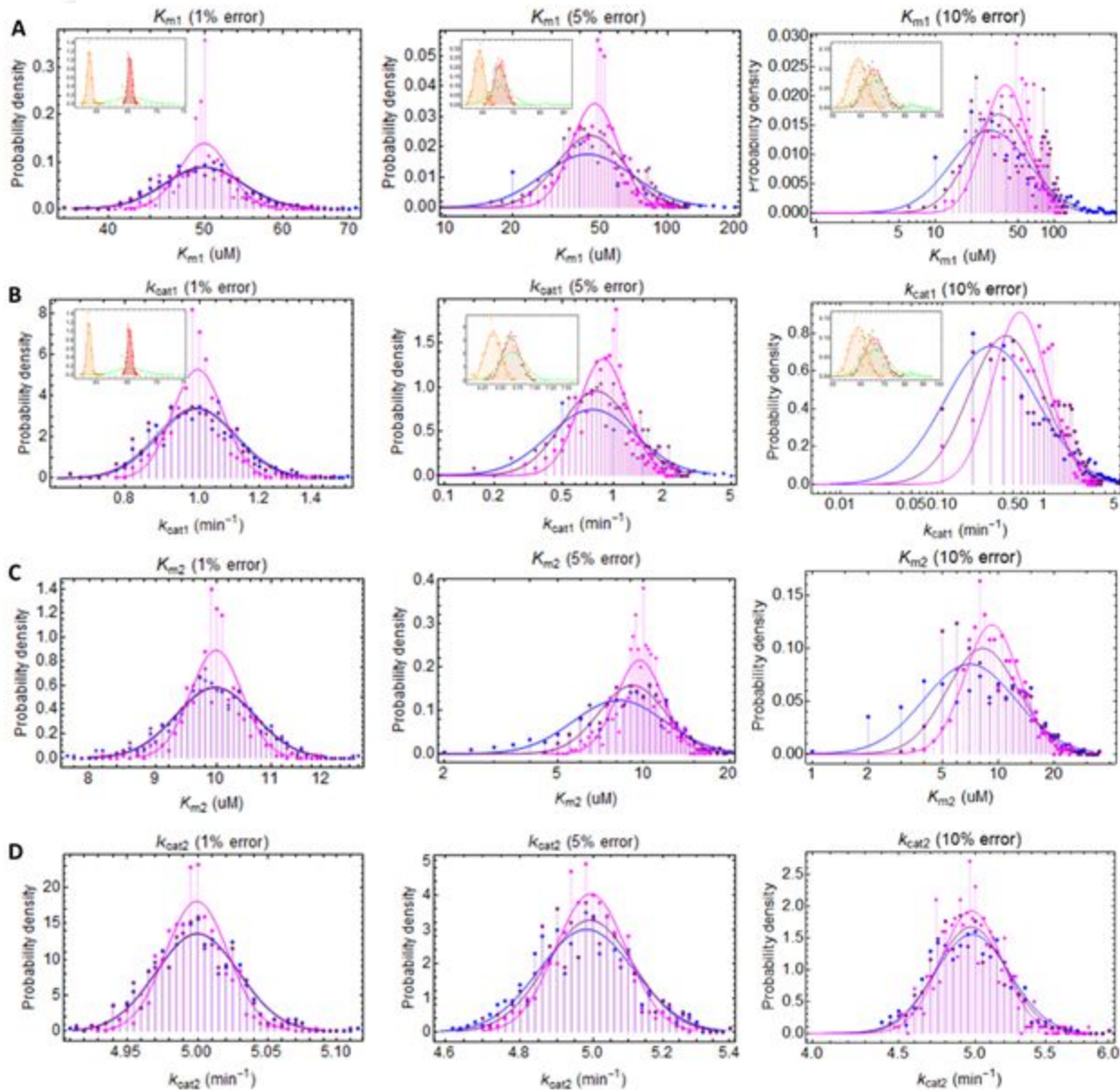
Figure 7.
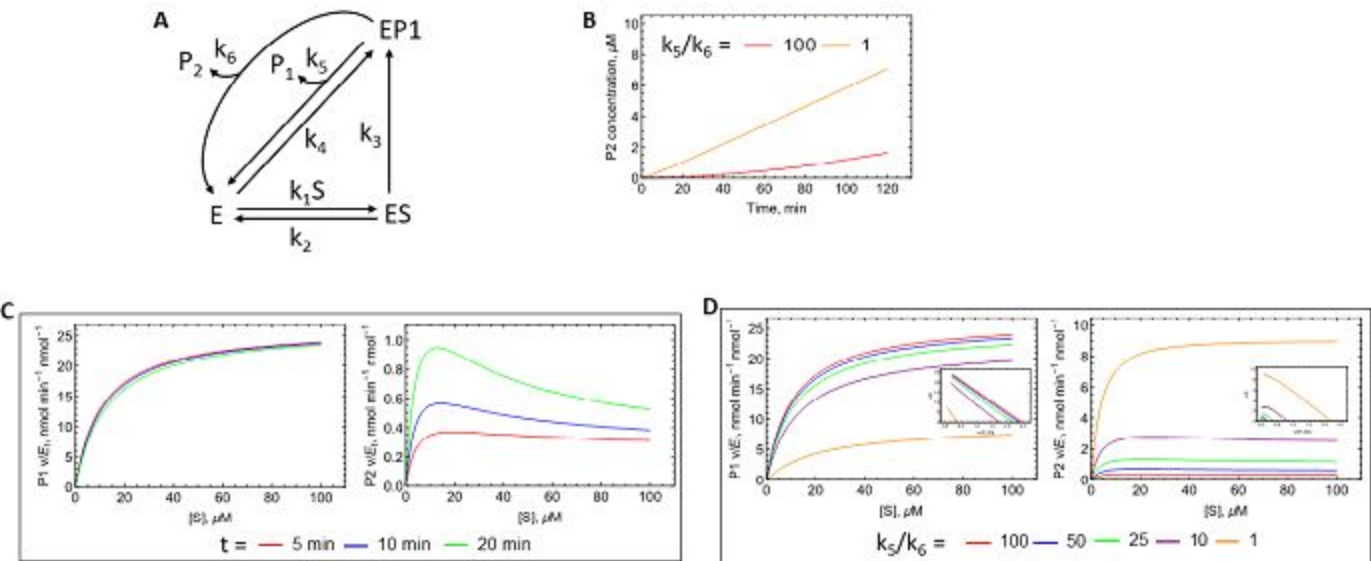
Figure 8.

Figure 9.

Figure 10.